Electronic Supplementary Material (ESI) for Nanoscale.

Supplementary Information

Room Temperature Ferroelectricity and Electrically Tunable Berry Curvature Dipole in III-V Monolayers

Ateeb Naseer,[*,†] Achintya Priydarshi,[*,†] Pritam Ghosh,[‡] Raihan Ahammed,[¶] Yogesh Singh Chauhan,[*,†] Somnath Bhowmick,[*,‡] and Amit Agarwal[*,¶]

†*Department of Electrical Engineering, Indian Institute of Technology, Kanpur, Kanpur 208016, India*

‡*Department of Materials Science & Engineering, Indian Institute of Technology, Kanpur, Kanpur 208016, India*

¶*Department of Physics, Indian Institute of Technology, Kanpur, Kanpur 208016, India*

E-mail: ateeb20@iitk.ac.in; achintya@iitk.ac.in; chauhan@iitk.ac.in; bsomnath@iitk.ac.in; amitag@iitk.ac.in

Table S1: Table of calculated lattice constants and optimum buckling height

Compound	Lattice constant (Å)	Buckling height (Å)
InP	4.1675	0.5599
InAs	4.2960	0.7069
InSb	4.6056	0.8032
GaAs	4.0079	0.6137
GaP	3.8628	0.4261
AlSb	4.3477	0.6745

Phonon and Phonon modes

The phonon spectra are examined in order to validate the dynamic stability of the freestanding buckled monolayers. It is observed that three acoustical modes and three optical modes exist. The absence of imaginary frequencies in the phonon dispersions confirms structural stability. Additionally, we calculate the phonon modes of the III-V monolayers to confirm the spontaneous polarization's alignment in the out-of-plane direction (see. Fig. S1).

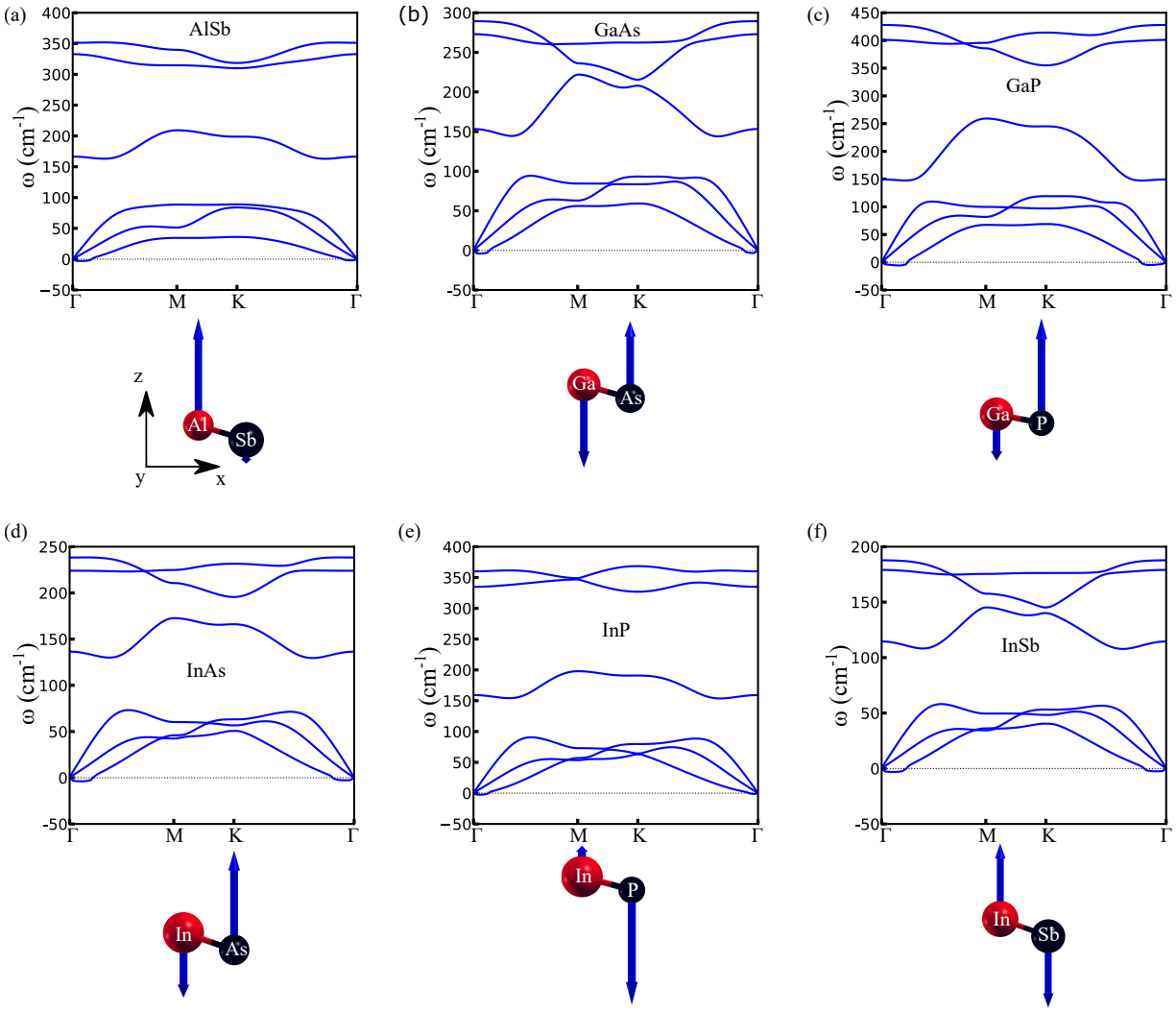

Figure S1: Phonon dispersions and polar vibrational modes responsible for spontaneous polarization of (a) AlSb, (b) GaAs, (c) GaP, (d) InAs, (e) InP, and (f) InSb monolayers.

Band Structrues

Fig. S2-S4 display the electronic bandstructures of all the III-V monolayers examined in this study along the high symmetry path of Γ-K-M-Γ. All the AB monolayers exhibit insulating properties, with all being direct bandgap except for the GaP.

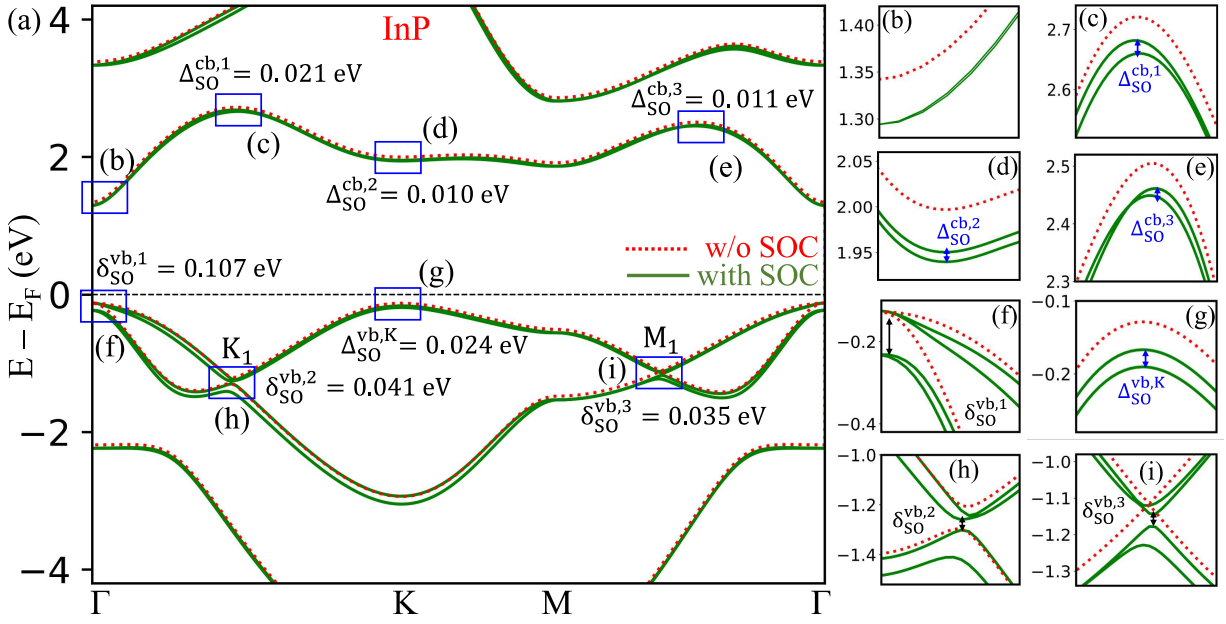

Figure S2: Spin-orbit splitted bands: (a) Electronic band structure of InP monolayer with (solid green line) and without (red dotted line) spin-orbit coupling (SOC). An enlarged view of spin-orbit splitted bands is depicted in (b-i) as indicated in (a).

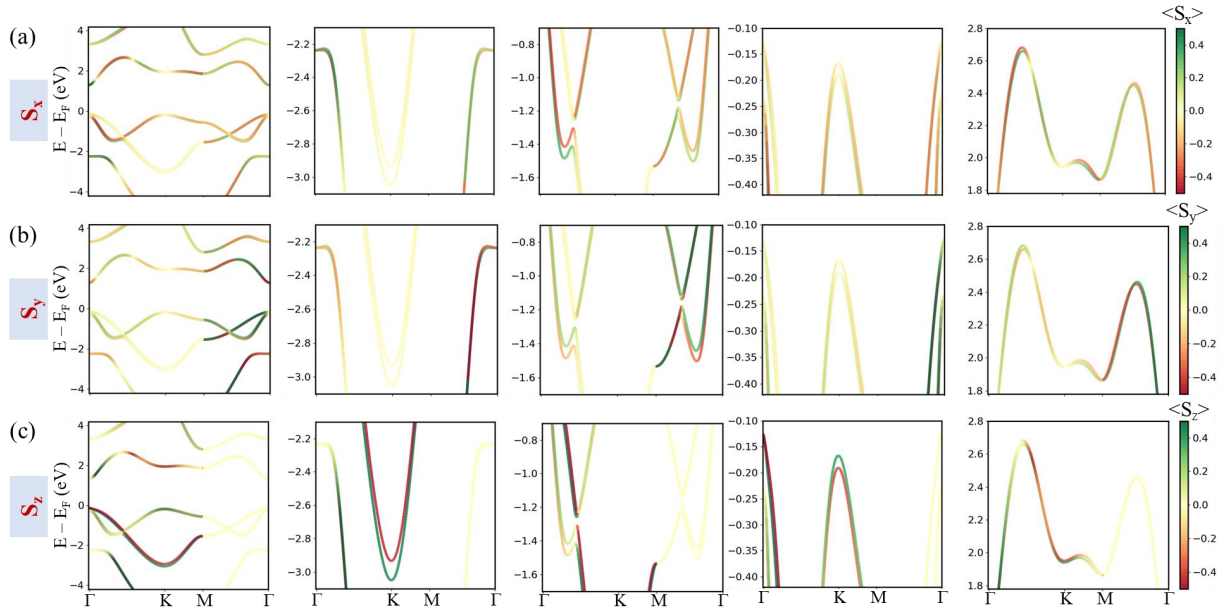

Figure S3: Spin projected band structure of InP monolayer. The color bar represents the spin expectation value.

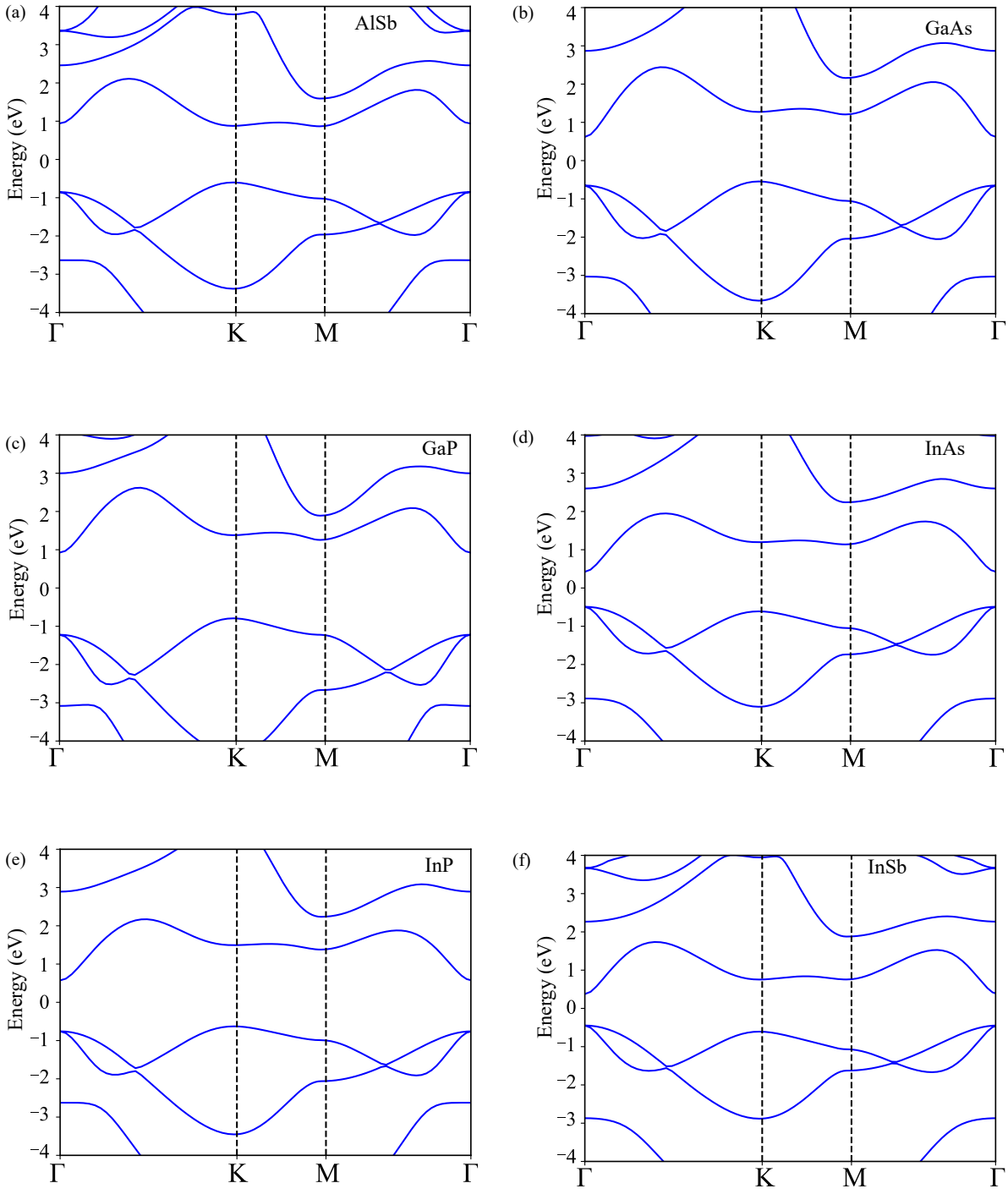

Figure S4: The electronic bandstructure for all III-V monolayers, (a) AlSb, (b) GaAs, (c) GaP, (d) InAs, (e) InP, and (f) InSb, in the polarized, buckled state.

Landau fitting curves

The transition from a non-centrosymmetric ferroelectric state to a centrosymmetric paraelectric state is achieved by small increments in the fraction of buckling height. The transition causes the out-of-plane polarization to shift from $\pm P_s$ to 0. The double well structures, free energy vs. δ and free energy vs. polarization, obtained using the Berry Phase method, show the transition from the ferroelectric state to paraelectric state and back to the ferroelectric state [see Fig. S5 and Fig. S6].

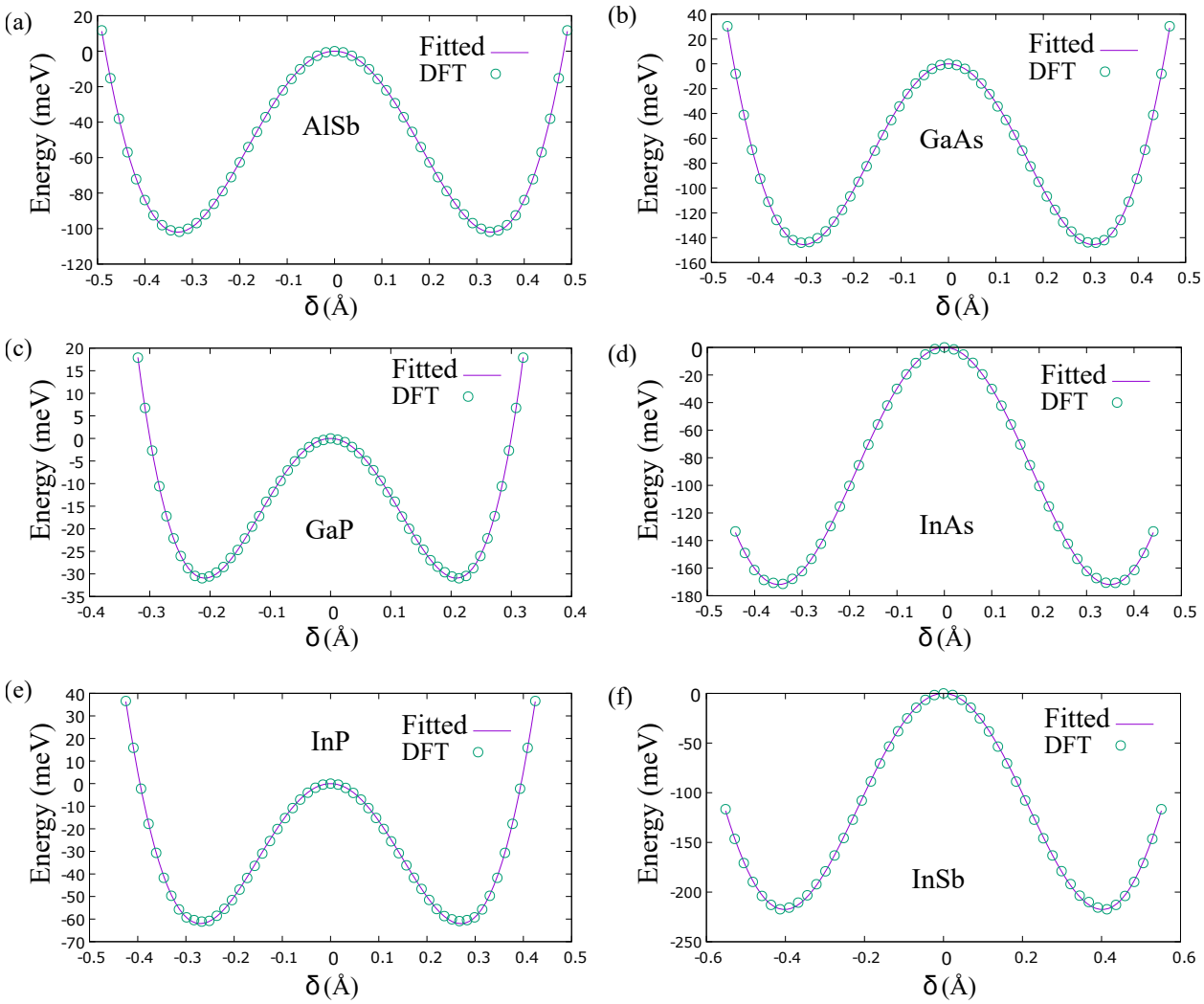

Figure S5: The DFT data for the dependence of the free energy on the buckling height (δ) for (a) AlSb, (b) GaAs, (c) GaP, (d) InAs, (e) InP, and (f) InSb fitted using a Landau Polynomial.

The Landau-Ginzburg (LG) theory is a mathematical framework for representing and analyzing continuous phase transitions. The energy transition of the system exhibits continuous behavior while the symmetry undergoes a discontinuous change. Within the framework of Landau-Ginzburg theory, the free energy can be mathematically represented as a Taylor series expansion centered around the order parameter (denoted as P) close to the transition point. The terms that fulfill the enhanced symmetries of the structure are preserved. Consequently, the free energy will solely depend on even powers of the order parameter. The fitting constants (A, B, and C) are determined by fitting the free energy data versus polarization obtained from density functional theory (DFT) with the Landau polynomial up to the sixth order.

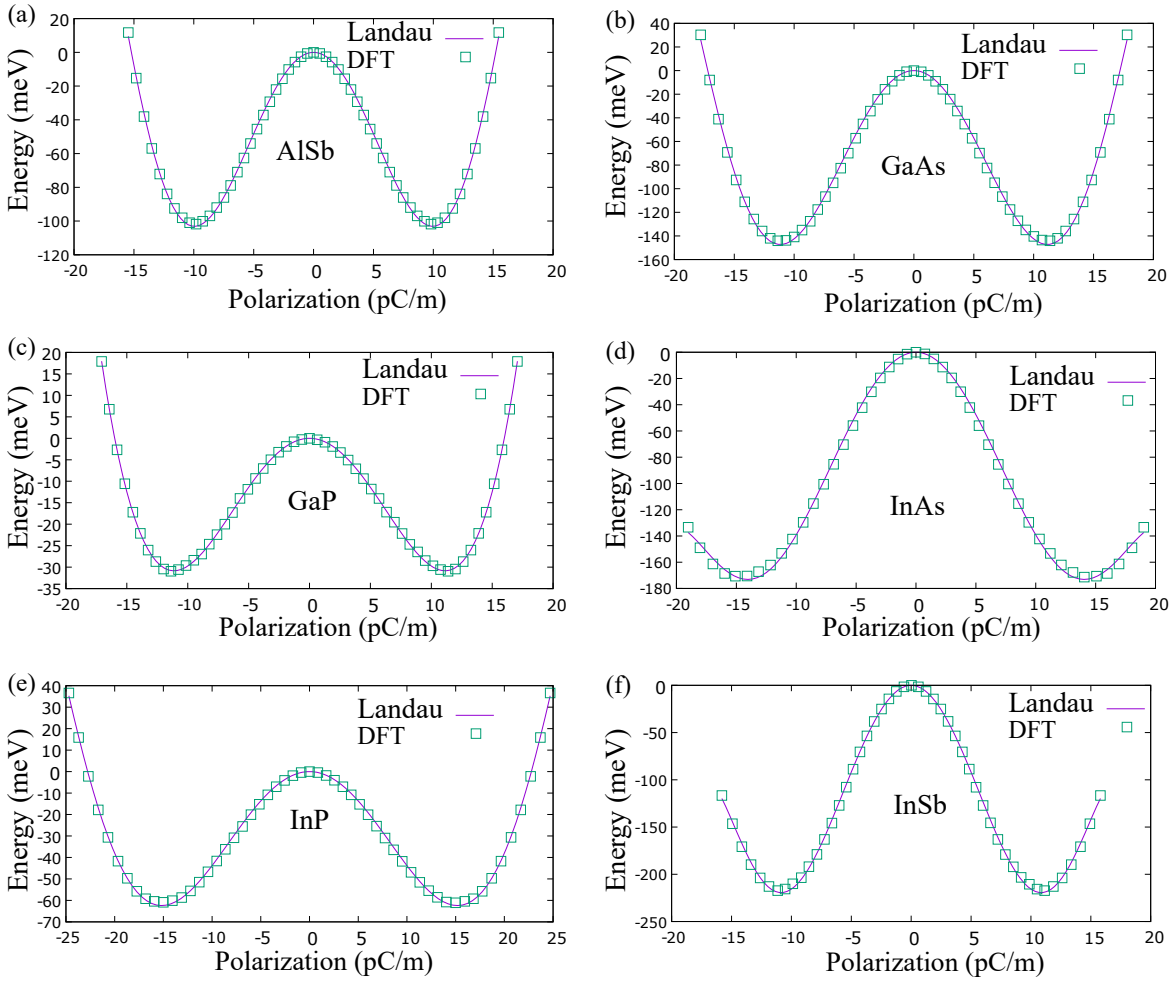

Figure S6: The DFT data for the variation in free energy with polarization for (a) AlSb, (b) GaAs, (c) GaP, (d) InAs, (e) InP, and (f) InSb fitted using a Landau Polynomial.

Table S2: The out-of-plane spontaneous polarization values for various reported 2D materials. InP outperforms most of the materials in terms of P_s [$\sim$ 13.96 (pC/m)] or effective bulk polarization of $\sim$ 2.79 (μC/cm^2) assuming an approximate layer thickness of 0.5 nm.[1]

Material	P_s	Units	Ref.
$MoTe_2$	0.10	(μC/cm^2)	[2]
WTe_2	0.11	(μC/cm^2)	[2]
$MoSe_2$	0.15	(μC/cm^2)	[2]
WS_2	0.18	(μC/cm^2)	[2]
WSe_2	0.21	(μC/cm^2)	[2]
MoS_2	0.23	(μC/cm^2)	[2]
$CuInP_2S_6$	4.0	(μC/cm^2)	[3]
PbSe	5.0	(μC/cm^2)	[4]
PbS	5.5	(μC/cm^2)	[4]
InSe	0.24	(pC/m)	[5]
GaSe	0.46	(pC/m)	[5]
$CuVP_2Se_6$	0.65	(pC/m)	[6]
$CuCrP_2Se_6$	0.67	(pC/m)	[6]
$CuVP_2S_6$	0.78	(pC/m)	[6]
$CuCrP_2S_6$	0.79	(pC/m)	[6]
CrB_2	0.90	(pC/m)	[7]
$AgBiP_2Se_6$	1.2	(pC/m)	[8]
BN	2.08	(pC/m)	[5]
SiC	6.17	(pC/m)	[5]
ZnO	8.22	(pC/m)	[5]
GaN	9.72	(pC/m)	[5]
AlN	10.29	(pC/m)	[5]
α-In_2Se_3	11.0	(pC/m)	[9]

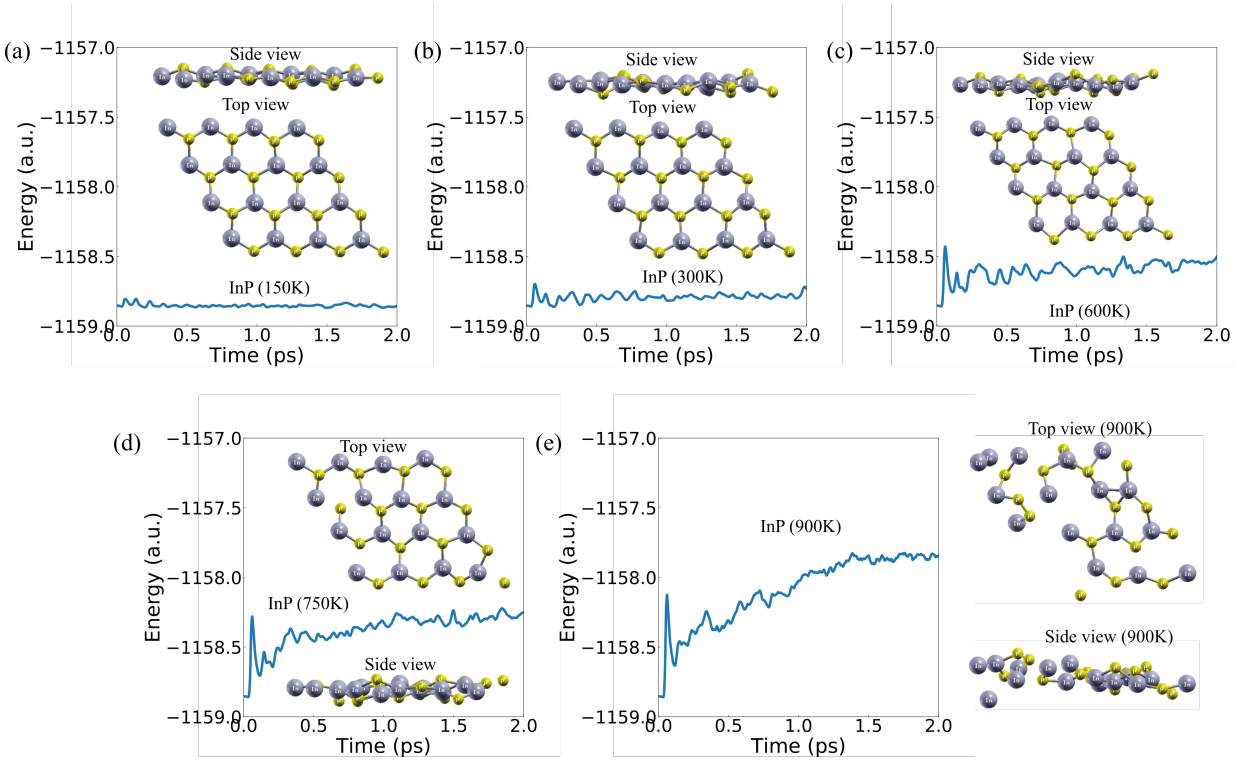

Figure S7: Energy variation for different temperatures (a) 150K, (b) 300K, (c) 600K, (d) 750K, and (e) 900K for monolayer InP. The insets present the top and side views at various temperatures. The monolayer is distorted at 750 K and breaks completely at 900 K.

Ferroelectric tunnel junction

The values of the left/right electrode screening length and dielectric permittivity for each simulation are as follows: $\delta_L = 0.07$ nm, $\delta_R = 0.24$ nm, $\epsilon_L = \epsilon_0$, and $\epsilon_R = 10\ \epsilon_0$.[10] The fixed rectangular barrier height (U_0) is taken to be 0.5 eV.[11,12]

Table S3: Table of the effective mass of electrons and holes, the relative dielectric constant of ferroelectric, effective bulk polarization.

Material	m_e	m_h	ϵ_{FE} (ϵ_0)	P_s (μC/cm^2)
InP	0.1064	0.7616	12.40	2.79
InAs	0.0791	0.5996	15.13	2.73
InSb	0.0675	0.5293	17.12	2.01
GaAs	0.0796	0.5703	13.18	1.97
GaP	0.1104	0.6811	11.11	2.04
AlSb	0.3706	0.5262	11.63	1.96

References

(1) Fei, R.; Kang, W.; Yang, L. Ferroelectricity and Phase Transitions in Monolayer Group-IV Monochalcogenides. *Phys. Rev. Lett.* **2016**, *117*, 097601.

(2) Bruyer, E.; Di Sante, D.; Barone, P.; Stroppa, A.; Whangbo, M.-H.; Picozzi, S. Possibility of combining ferroelectricity and Rashba-like spin splitting in monolayers of the 1T-type transition-metal dichalcogenides MX_2(M=Mo,W;X=S,Se,Te). *Phys. Rev. B* **2016**, *94*, 195402.

(3) You, L.; Zhang, Y.; Zhou, S.; Chaturvedi, A.; Morris, S. A.; Liu, F.; Chang, L.; Ichinose, D.; Funakubo, H.; Hu, W.; Wu, T.; Liu, Z.; Dong, S.; Wang, J. Origin of giant negative piezoelectricity in a layered van der Waals ferroelectric. *Science Advances* **2019**, *5*, eaav3780.

(4) Hanakata, P. Z.; Rodin, A. S.; Park, H. S.; Campbell, D. K.; Castro Neto, A. H.

Strain-induced gauge and Rashba fields in ferroelectric Rashba lead chalcogenide PbX monolayers (X = S, Se, Te). *Phys. Rev. B* **2018**, *97*, 235312.

(5) Li, L.; Wu, M. Binary Compound Bilayer and Multilayer with Vertical Polarizations: Two-Dimensional Ferroelectrics, Multiferroics, and Nanogenerators. *ACS Nano* **2017**, *11*, 6382–6388.

(6) Qi, J.; Wang, H.; Chen, X.; Qian, X. Two-dimensional multiferroic semiconductors with coexisting ferroelectricity and ferromagnetism. *Applied Physics Letters* **2018**, *113*, 043102.

(7) Luo, W.; Xu, K.; Xiang, H. Two-dimensional hyperferroelectric metals: A different route to ferromagnetic-ferroelectric multiferroics. *Phys. Rev. B* **2017**, *96*, 235415.

(8) Xu, B.; Xiang, H.; Xia, Y.; Jiang, K.; Wan, X.; He, J.; Yin, J.; Liu, Z. Monolayer $AgBiP_2Se_6$: an atomically thin ferroelectric semiconductor with out-plane polarization. *Nanoscale* **2017**, *9*, 8427–8434.

(9) Soleimani, M.; Pourfath, M. Ferroelectricity and phase transitions in In_2Se_3 van der Waals material. *Nanoscale* **2020**, *12*, 22688–22697.

(10) Velev, J. P.; Burton, J. D.; Zhuravlev, M. Y.; Tsymbal, E. Y. Predictive modelling of ferroelectric tunnel junctions. *npj Computational Materials* **2016**, *2*, 16009.

(11) Rodrıguez Contreras, J.; Kohlstedt, H.; Poppe, U.; Waser, R.; Buchal, C.; Pertsev, N. A. Resistive switching in metal–ferroelectric–metal junctions. *Applied Physics Letters* **2003**, *83*, 4595–4597.

(12) Zhuravlev, M. Y.; Sabirianov, R. F.; Jaswal, S. S.; Tsymbal, E. Y. Giant Electroresistance in Ferroelectric Tunnel Junctions. *Phys. Rev. Lett.* **2005**, *94*, 246802.